Engineering Geology 244 (2018) 107–115

Contents lists available at ScienceDirect

Engineering Geology

journal homepage: www.elsevier.com/locate/enggeo

Rotational–translational landslides in the neogene basins at the northeast margin of the Tibetan Plateau

Peng Xin[a], Zhen Liu[b,*], Shu-ren Wu[a], Changyu Liang[a], Cheng Lin[c]

[a] Key Laboratory of Neotectonic Movement and Geohazard, Ministry of Land and Resources, Institute of Geomechanics, Chinese Academy of Geological Science, Beijing 100081, China
[b] Department of Civil & Environmental Engineering, Louisiana State University, Baton Rouge, LA 70803, United States
[c] Department of Civil Engineering, University of Victoria, Victoria, BC V8P 5C2, Canada

ARTICLE INFO

Keywords:
Neogene
Tibetan Plateau
Geomorphology
Landslide
Rotational–translational

ABSTRACT

Rotational–translational landslides are common in Neogene basins throughout the world and are of high risk to the public. To understand the mechanism of rotational–translational failure, the spatial distribution and deformation of rotational–translational landslides in the northeast of the Tibetan Plateau are investigated in this study. The spatial distribution of these landslides is dependent on the regional tectonics and geomorphology, crustal stresses, and lithological properties. The rotational–translational landslides are concentrated in the Neogene mudstone basins, and the intensities of these landslides are observed to gradually decrease from the hinterland of the plateau to the marginal basins. The bedding-parallel shear zones within the location of the rotational–translational landslides are present in the overconsolidated Neogene mudstones with high clay content. Nearly horizontal tectonic stresses and erosion cause the formation of horizontal shear stresses in the sliding masses. In this stress environment, materials with low internal friction angle ($< 10^{\circ}$) are observed to develop in the shear zones. A weak layer with high clay content and low calcium content are observed in all the bedding-parallel shear zones of rotational-translational landslides. Further, illite–montmorillonite and illite are the main clay minerals of all the shear zones with no montmorillonite. Horizontal shearing is further accelerated by increasing the pore-water pressure and creep.

1. Introduction

Rotational–translational landslides are common in Neogene basins throughout the world (Di Maio et al., 2010, 2013; Haruo, 2001; Yenes et al., 2009, 2015). They are typically characterized with arc-shaped sliding faces in the back and the nearly bedding-parallel shear zones in the front and middle. The Neogene claystone basins in the northeastern margin of the Qinghai–Tibet Plateau contain several rotational–-translational landslides that pose significant risk to both infrastructure and humans. Failures include the huge ancient Zhangjiazhuang landslide in Ludu County, which is located at the Xining Basin in the upper reaches of the Yellow River. The landslide was gradually activated and failed on January 18, 2016. It terminated the operation of the Lanzhou–Xinjiang high-speed rail for almost six months. The Sale Mountain landslide in the Linxia Basin in 1983 caused 273 injuries and deaths. Another landslide that had a volume of 800×10^4 m^3 occurred at the Huaxu Village of the Lantian County and destroyed several residences.

It is generally known that the development and rotation of the arc-shaped sliding plane at the trailing edge of a landslide body satisfies the Mohr–Coulomb failure criterion and that the formation of a rotational–translational landslide can be controlled by the bedding-parallel shear zones with nearly horizontal sliding surfaces (Varnes, 1978). The triggering of bedding-parallel shearing requires low internal friction angles of 0°–10° and horizontally distributed shear stress. Skempton (1964, 1985) observed that repeated shearing usually causes internal friction angles of 5°, 10°, and 15° for pure montmorillonite, illite, and kaolinite, respectively. There are three possible explanations for the development of horizontal stresses. First, bedding-parallel shearing is observed to typically occur because of the presence of weak layers or the development of plastic sliding zones owing to the stress concentration in the weak layers near the sliding surface (Hart, 2000; Massey et al., 2013, 2016; Petley et al., 2002; Wen and Aydin, 2003). Second, extensive and deep erosion can reach hundreds of meters, which causes significant unloading of overconsolidated claystone and stress redistribution in river gullies (Palladino and Peck, 1972). Third, the gravitational creep and strong expansion or shrinkage in claystone

* Corresponding author.
E-mail addresses: zhenliu.ce@gmail.com, zhen.liu@terracon.com (Z. Liu).

https://doi.org/10.1016/j.enggeo.2018.07.024
Received 5 February 2018; Received in revised form 25 July 2018; Accepted 30 July 2018
Available online 01 August 2018
0013-7952/

could induce failure (Carey and Petley, 2014), as reported for the Boqishan landslide (Xin et al., 2016).

In order to examine the mechanisms of the landslides in the Qinghai–Tibet Plateau and the cause behind the frequent landslides in this area, this study presents the measured deformation in the bedding-parallel shear zones and addresses the following queries: (1) What is the spatial distribution of the rotational–translational landslides at the northeastern margin of the Tibetan Plateau? (2) What is the geometry of the bedding-parallel shear zone(s) during rotational–translational landslides? (3) What are the deformation mechanisms and the triggering-shearing factors of the bedding-parallel shear zone(s)?

2. Temporal and spatial distribution of the rotational–translational landslides

The rotational–translational landslides are concentrated at the northeast margin of the Qinghai–Tibet Plateau. > 87 rotational–-translational landslides are observed in the study area, the majority of which are located along the banks of large valleys in the Neogene claystone basins, e.g., the Yellow River and Wei River or their tributaries and the Hulu River (Zhang et al., 2017a, 2017b, 2018). The landforms control the volume of landslides. As illustrated in Fig. 1, the sizes of the landslides decrease with elevation from west to east. Giant landslides that have volumes of $> 1 \times 10^8\ m^3$ are common in the high-elevation terrain in the upstream of the Yellow River at 2000–3500 m above sea level and at relief of 300–500 m. Large-scale landslides that have volumes of $> 1 \times 10^7\ m^3$ are common in the Wei River at 1500–2500 m above sea level and at relief of 200–300 m. Medium-sized landslides exhibit volumes of approximately $1 \times 10^6\ m^3$ and are common in the lower region of the Wei River between 300 and 900 m above the sea level. In this area, the size of the erosion landforms gradually decreases, covering a height of approximately 180 m.

Giant landslides are mainly distributed in the valleys at the upper reaches of the Yellow River drainage system, primarily in Gonghe, Guide, Xunhua, and Xining Basins. > 32 landslides exhibit volumes of $> 1 \times 10^8\ m^3$. For example, the volume of the 1954 Chana landslide in Gonghe Basin was $1.2 \times 10^8\ m^3$. Ten landslides, including the Kangyang landslide, have occurred at the Jianzha Basin, which is the largest number of landslides that have occurred at any basin. The Canguotan landslide, for example, comprises a sliding body with a thickness of 35 m, width of 800 m, length of 1700 m, and volume of $4.7 \times 10^7\ m^3$. Its leading edge is the level III terrace of the Yellow River, and a 20-cm thick shear zone is present within the Neogene claystone between the sand and gravels. The central sliding surface is relatively flat with a dip angle of approximately 6° (Fig. 2a). The Xijitan landslide in the Guide Basin and the Xiazangtan landslide in the Gonghe Basin exhibit similar features. The Neogene claystone sliding surface of the Xiazangtan landslide is relatively flat, with a dip angle of 2°–8°.

Large-scale landslides are observed in the middle reaches of the Yellow River in the Longzhong Basin. There are 23 landslides that exhibit volumes of $> 1 \times 10^4\ m^3$, including the Sale Mountain landslide and the landslides at the north slope of the Tianshui City. The sliding surface of the Sale Mountain landslide along the Baxie River cuts through the 120-m thick loess deposits and a nearly horizontal Neogene mudstone, and an easement curve connects the middle parts, as depicted in Fig. 2b. The Panan Town landslide in the Wei River Valley was triggered by an M7 earthquake. It has an east–west width of approximately 4.7 km, a north–south length of approximately 3.1 km, and a thickness of 104 m. The back wall is almost 70° steep, whereas the middle and back edge are relatively flat with a dip angle of 6°–10°. Similar cases are the landslides at Wangjiayao, Qinan County and the landslides at the northern bank of the Tianshui City.

Medium-sized landslides are observed along the northern bank of the middle and lower reaches of the Wei River Basin. Thirty-five landslides have occurred in the area and have repeatedly claimed lives, for example, Wolong Temple landslide, the landslide in Nanshetou, and the Caijiapo landslide depicted in Fig. 2c. The landslide in Xujiacun, for example (Fig. 2d), exhibits a nearly horizontal clay sliding surface at the center that extends 500 m with a dipping angle of 6°–8°. The Caijiapo landslide is similar in form and deformation style.

3. Faulting along bedding and rotational–horizontal landslides

3.1. The geometric for rotational-horizontal landslide

The rotational–horizontal landslides comprise rotational slip zones and translational sliding zones (Yenes et al., 2009, 2015). As illustrated in Fig.3, the rotational slip zone is the trailing edge of the sliding body, and the rotational failure is attributed to stretching. Gravity is the main controlling factor in this zone. The translational sliding zone is located in the front and middle parts of the sliding body and is divided into three distinct stress and strain zones that are characterized by extension, translation, and contraction during shearing. Tectonic stress and the pore pressure of groundwater provide the horizontal shear stress in this zone (Lupini et al., 1981) that further produces the faults along the bedding.

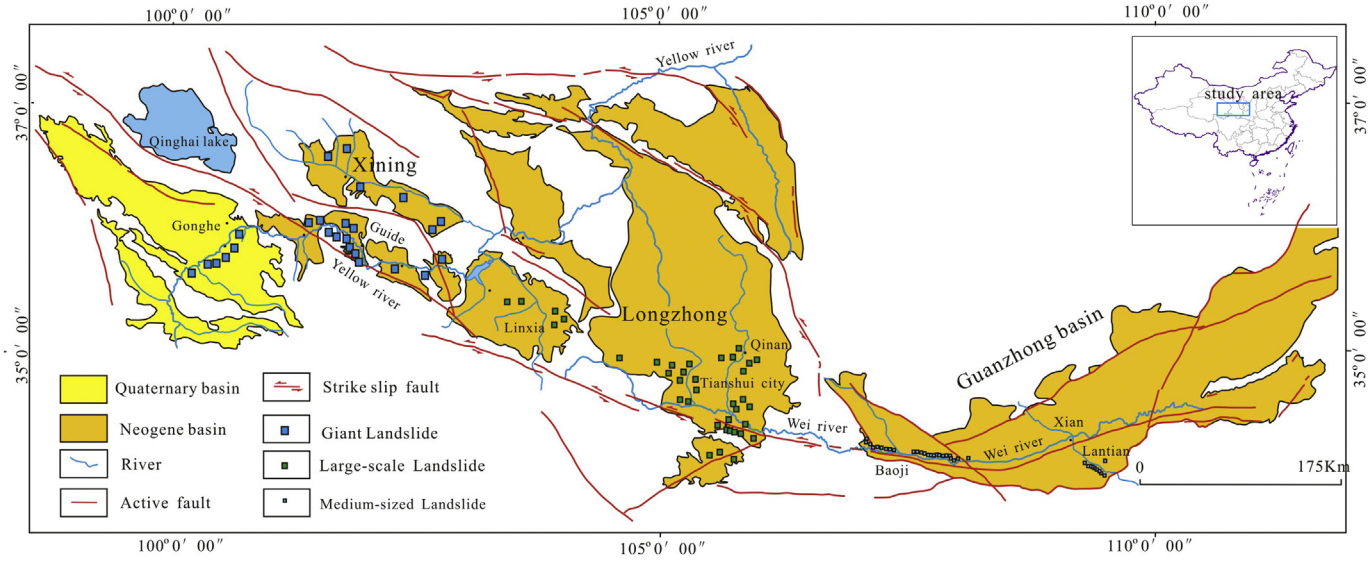

Fig. 1. Neogene claystone basins at the northeast margin of the Qinghai–Tibet Plateau and the distribution of rotational–translational landslides.

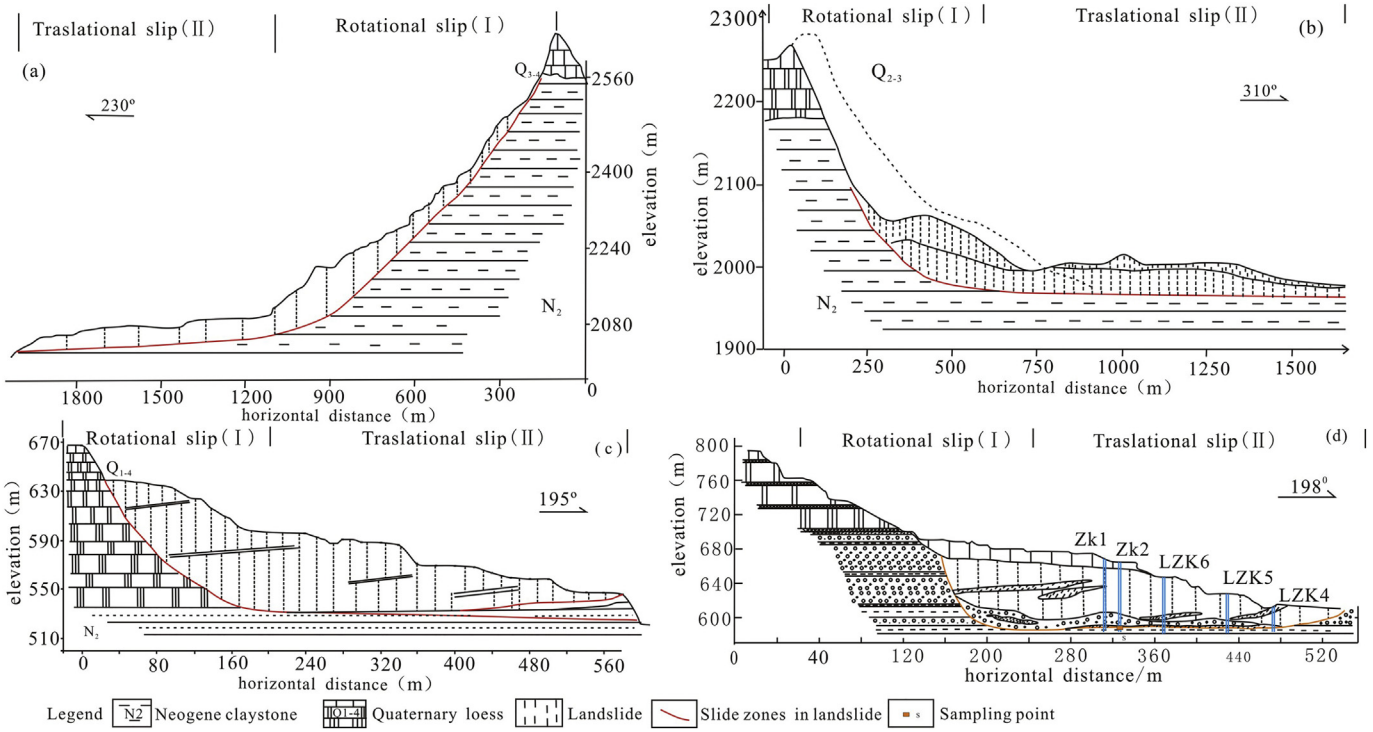

Fig. 2. Cross-sections of the rotational–translational landslides. (a) Canguotan landslide in the Jianzha Basin; (b) Saleshan landslide in the Longzhong Basin; (c) Caijiapo landslide in the Wei River Basin; and (d) Bojishan landslide in the Wei River Basin.

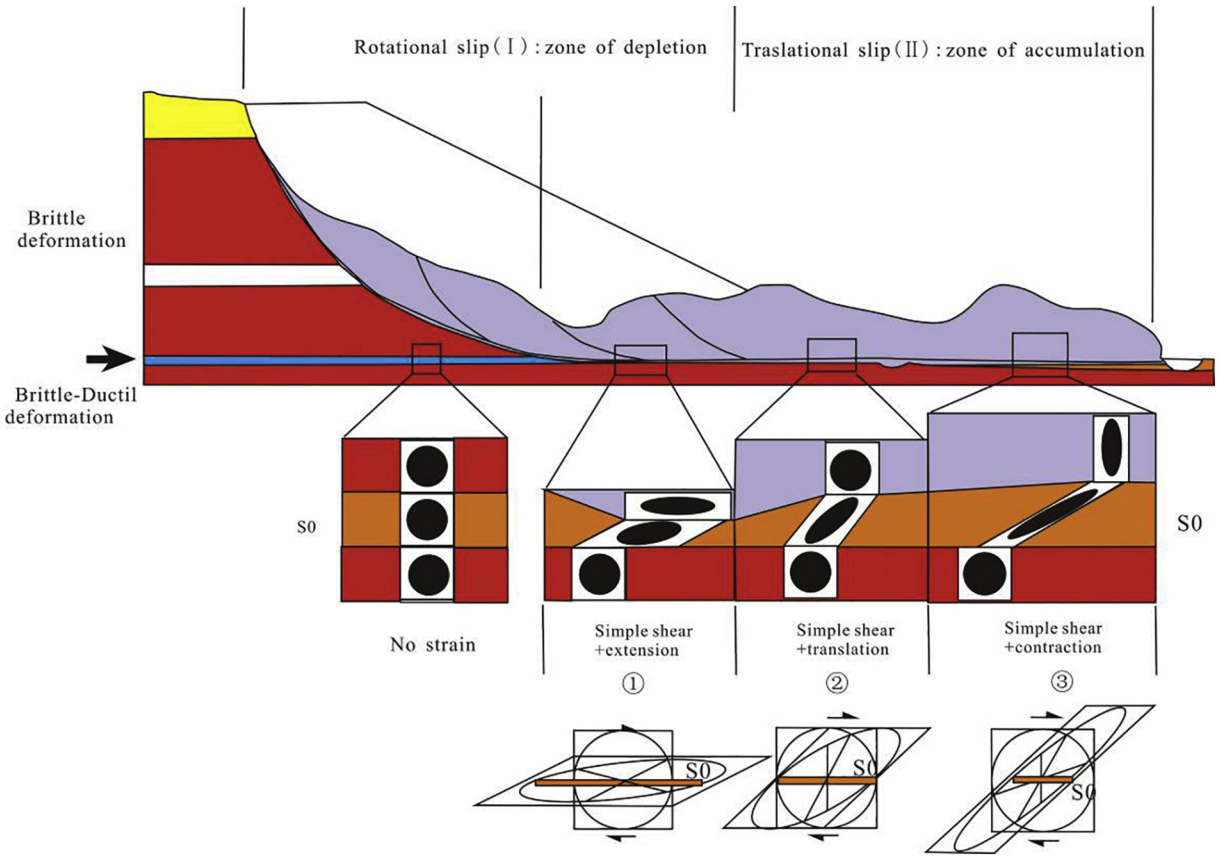

Fig. 3. Geometric and strain model of rotational-translational landslides (Yenes et al., 2009).

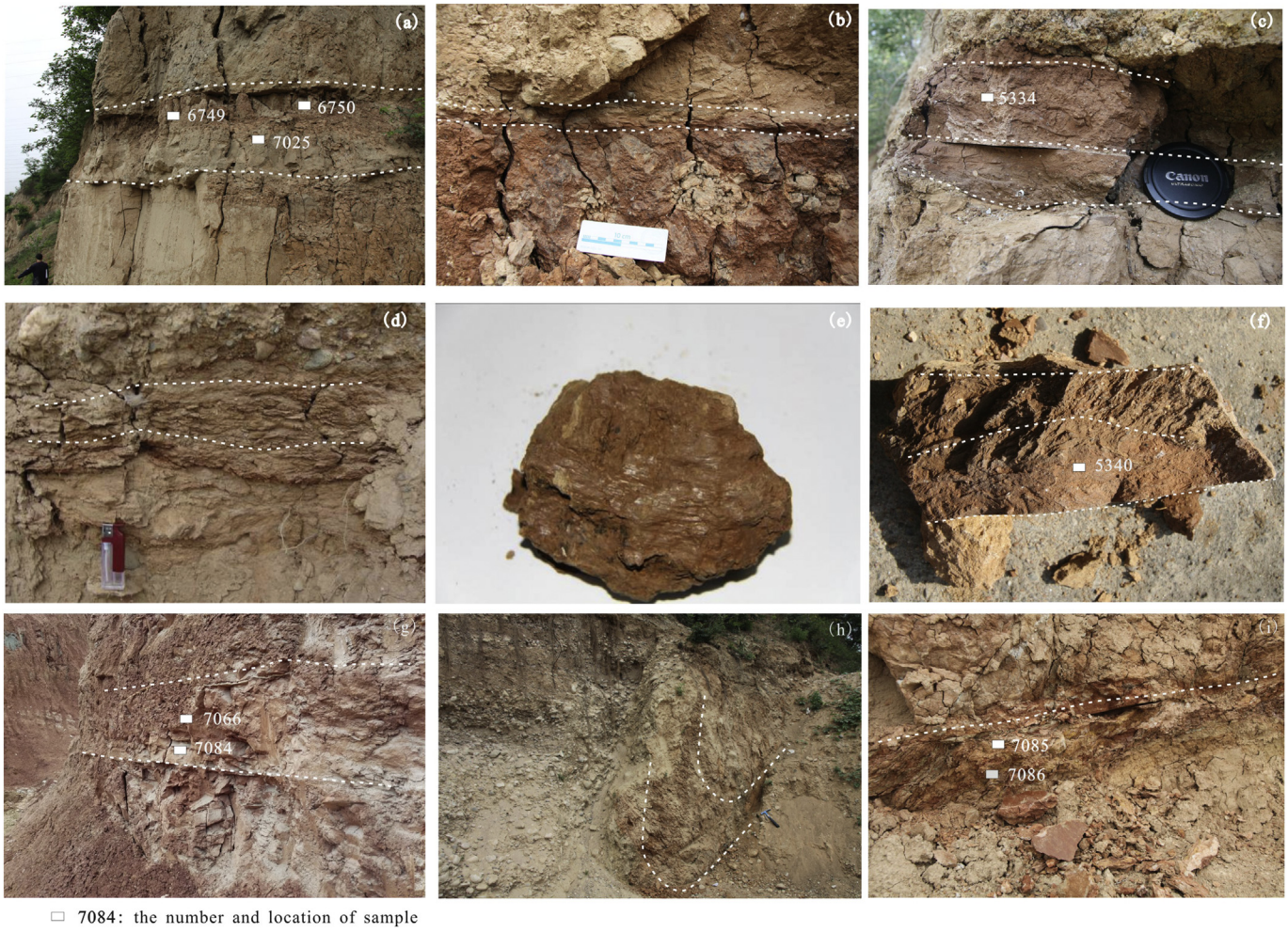

Fig. 4. Ductile and brittle deformation in typical sliding zones (a) Caijiapo landslide; (b) Tongjiapo landslide; (c) Gaojiaya landslide; (d) Xiazangtan landslide; (e) Bojishan landslide; (f) Gaojiaya landslide and ductile deformation; (g) Gaojiawan landslide; (h) Dianzijie landslide; and (i) Panan landslide.

3.2. Faulting along the bedding in horizontal shear zones

In the translational shear zone, the shear localization in the claystone causes the random alignment of particles. These shear bands are clay-rich and exhibit a friction angle of $< 10^{\circ}$ (Skempton, 1985; Kimuta et al., 2018). The shear stress exerted on the shear bands is higher than the friction that is required to orient the particles, which causes creep or the rapid abrasion of clay particles and a change from the original flocculent structure to a layered structure. For example, the shear zone in the Caijiapo landslide is 40 cm thick and is controlled by two approximately parallel sliding surfaces (Fig. 4a). However, the main sliding band in the middle of the Tongjiapo landslide is only about 5 cm thick, with clear orientation of clay minerals (Fig. 4b). Ductile deformation dominates, as indicated by the Gaojiaya landslide in Fig. 4c and the Xiazangtan landslide in Fig. 4d, despite the fragmentation being attributed to brittle deformation. Fig. 4e exhibits the specimens from the Bojishan landslide in which the main sliding band depicts a layered horizontal structure. Plastic deformation, cleavage, and microfolds are observed in the clay-rich shear zones (Fig. 4f). The translational shear zones of the Guojiashan landslide in the Xining Basin exhibit similar features to those depicted in Fig. 4g.

In the contractional shear zone, there is evidence for strong and multistage deformation, such as the plastic extrusion of mudstone and claystone (Fig. 4h). The clay layers exhibit strong plastic deformation, whereas the stone layers are nearly vertical and exhibit evidence for plastic extrusion. In the Panan landslide, the original mudstone is approximately 0.8 m thick (Fig. 4i). Shearing thins the mudstone to form 0.2-m thick bands. Fracture shearing is observed in the red claystone layers, and plastic deformation in the claystone layers.

3.3. Deformation and groundwater fluctuations in landslides

Groundwater fluctuation accelerates the creep in landslides. Fig. 4 exhibits the pore-water pressure and deformation data for the Bojishan landslide since 2012. The sliding zone of the landslide is 12.3 m thick and comprises the main sliding zone and a jointed zone. The clay-rich soil in the jointed zone, where the No. 1 and No. 4 inclinometers are located, is heavily fragmented. The main sliding zone, where the No. 1 and No. 4 inclinometers are located, has been continuously deforming for several years. The displacement on the slip surface has been monitored since 2012 using four inclinometers (Fig. 5a). Inclinometer No. 1 did not record any deformation. The maximum deformation of 16.53 mm is observed along a shear zone near inclinometer No. 2. The fluctuation of the groundwater level causes the landslide to move, and the slip rate correlates with the pore-water pressure. The data indicate that the pore-water pressure fluctuates, with an average of 92 kPa, and the lowest value is observed between January and May (Fig. 5b). During the rainy season from June to October, the amount and strength of rainfall is high; consequently, the water pressure increases from 90 to 96 kPa. This is followed by a decrease in the water pressure owing to the low frequency and intensity of rainfall after October. From August 1 to 31, 2012, the pore-water pressure in the landslide increased from 93.1 to 95.3 kPa; further, inclinometer No. 3 recorded a significant displacement of 2–4 mm (Fig. 5c).

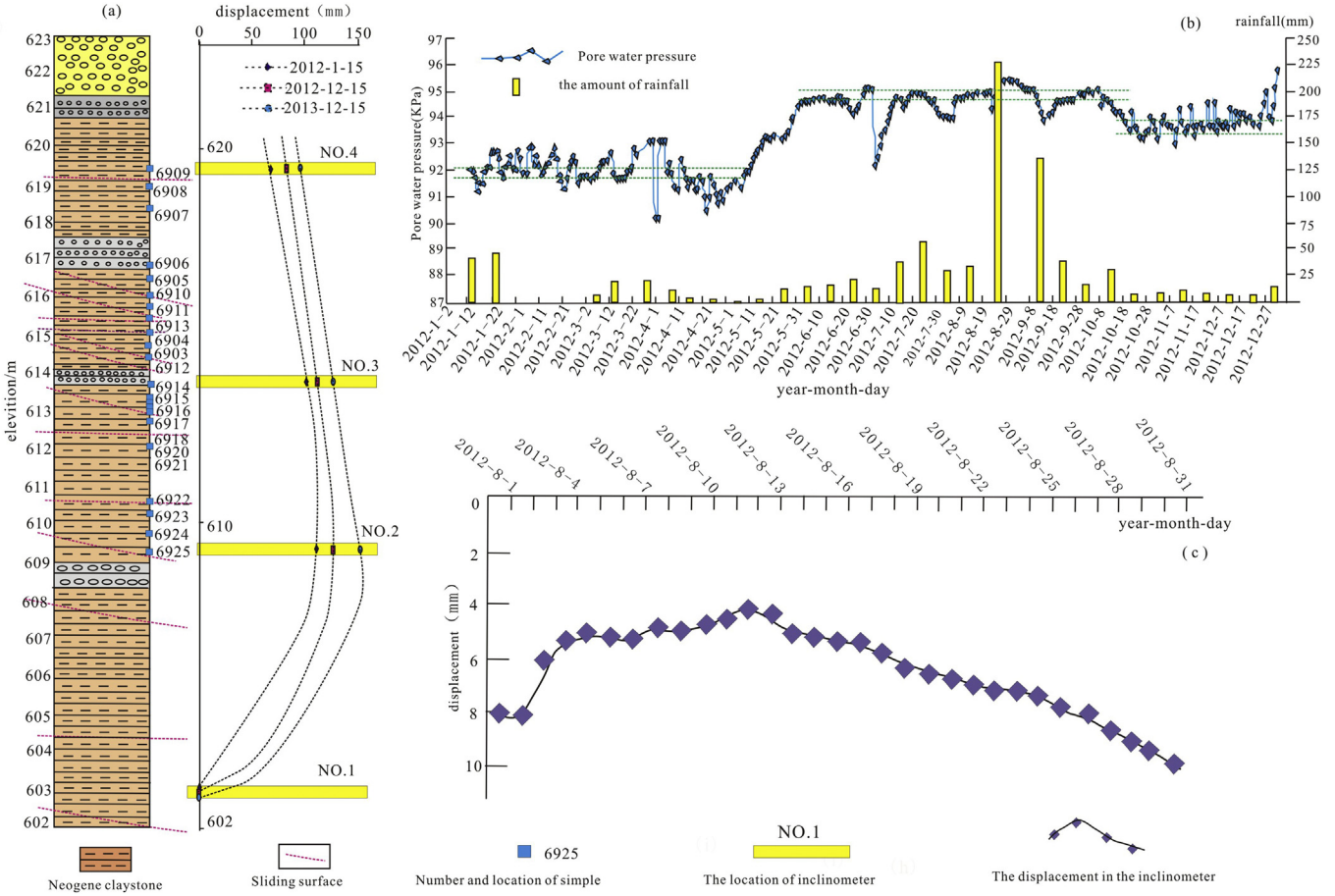

Fig. 5. Deformation due to the Bojishan landslide (a) Drilling and displacement monitoring in the Bojishan landslide; (b) pore-water pressure measurements in 2012; and (c) displacement of the No. 3 inclinometer in August 2012.

4. Physicochemical coupling in the horizontal shearing zone

The material composition of the shear zones plays a critical role in active landslides. Lupini et al. (1981) indicated that the mechanical properties of a landslide body are dependent on the structure and material composition of the shear zone and that viscous deformation will occur if the clay content exceeds 50%. Low-angle sliding in the translational deformation zone is caused due to gradual creep. However, several questions still remain unsolved. Is the sliding surface formed in the claystone layers because of the softening of claystone? what is the role of groundwater seepage? What is the effect of physicochemical coupling when the shear tress is horizontal and parallel to bedding?

4.1. Material composition and physical characteristics

The Neogene red mudstone covers the northeastern margin of the Qinghai–Tibet Plateau and exhibits a maximum depositional thickness of 300 m. The mudstone components are sand, calcium carbonates, clay, and silt. The high slip rate and creep alter the initial structure and material composition of the mudstone. The sliding zones of landslides within the Northeast Neogene Basin of the Tibetan Plateau were selected for testing. The slip zones of most of the landslides are covered by the landslide deposits. Table 1 presents the clay content of the claystone layers in the landslides, i.e., 21.89%–62.60% in Guanzhong Basin, 36.22%–65.23% in Longzhong Basin, and 33.04%–37.84% in the Xining Basin. Calcium carbonate is the cement in claystone. Most of the sliding zones (e.g., Caijiapo and Gaojiayan landslides) develop in bedding-parallel shear zones with high clay and low calcium carbonate contents. Extensive sliding surfaces in the Bojishan landslide are identified at altitudes of 615.5, 611.4, and 608 m with clay contents of 62.6%, 62.46%, and 42.44%, respectively (Fig. 6a). These values are much higher than the values that are observed in case of any other landslide. At the same locations, the calcium carbonate content is 1.36%, 1.38%, and 4.51%.

Clay particles exhibit a high water absorption capacity and activity. When soils or rocks contain > 20% clay-size fraction (i.e., < 2 μm), they tend to have a significantly high specific surface area, very low permeability, and strong water-holding capacity, as depicted in Fig.6a. It can be observed from Table 1 that illite–montmorillonite and illite are the main clay minerals in the shear zones, with no montmorillonite and only minor amount of kaolinite. When the content of clay minerals is 33.04%, the water absorption is 32.25% and the specific surface area is 149.08 m^2/g. However, when the content of clay minerals is 48.28%, the water absorption is 40.23% and the specific surface area becomes 162.18. Because the clays are illite–montmorillonite and the mudstone is susceptible to the wetting and drying cycles, appreciable expansion and shrinkage develop and cause a high cracking potential. Table 2 presents the main sliding zones that contain a high percentage of illite–montmorillonite, and the maximum percentage is observed to be 69%.

4.2. Water seepage and claystone

The development of small-angle shear fractures in the claystone owing to water seepage may be explained by the following mechanism. First, the gradual destruction of the overconsolidated mudstone creates cracks that open passages for water seepage. Second, cracks develop

Table 1
Neogene claystone properties.

Location	Landslide	Sampling number	Water absorption of dry rock (%)	Particle-size distribution (%)			Montmorillonite content (%)	Specific surface area (m^2/g)	Calcium carbonate content (%)	Liquid limit (%)	Plastic index (%)
				> 0.25 mm		< 0.002 mm					
Guanzhong Basin	Gaojiaya landslide	5334	–	3.6	74.51	21.89	18.87	168.10	8.16	43.42	22.96
		5340	–	0	72.40	27.60	7.00	108.00	2.00	36.47	17.11
	Caijiapo landslide	6749		0.20	49.44	50.36	25.29	211.09	11.00	57.22	29.43
		6750	–	0.50	59.70	39.80	25.29	211.09	4.77	46.42	22.78
		7025	50.67	0.30	65.62	34.08	23.23	240.99	8.16	47.74	20.36
	Bojishan landslide	6903	40.23	1.22	50.50	48.28	17.06	162.18	4.65	46.17	26.22
		6905	34.67	0.79	59.49	39.72	15.62	152.54	3.37	42.43	20.87
		6910		0.9	36.5	62.60	29.23	250.55	1.36	66.65	37.14
		6914		1.0	40.96	58.04	27.31	224.14	1.18	58.66	30.67
Longzhong Basin	Panan landslide	7085	–	1.13	34.28	64.59	14.32	44.602	6.48	–	–
		7086	–	1.01	59.12	39.87	13.26	82.604	19.05	–	–
	Saleshan landslide	7087	–	1.03	62.75	36.22	13.64	44.23	39.06		
		7088	–	1.13	33.64	65.23	14.37	42.82	13.71		
Xining Basin	Gaojiawan landslide	7066	29.77	0	62.16	37.84	16.75	170.87	11.40	–	–
		7084	32.25	0.9	66.06	33.04	12.40	149.08	8.15	–	–

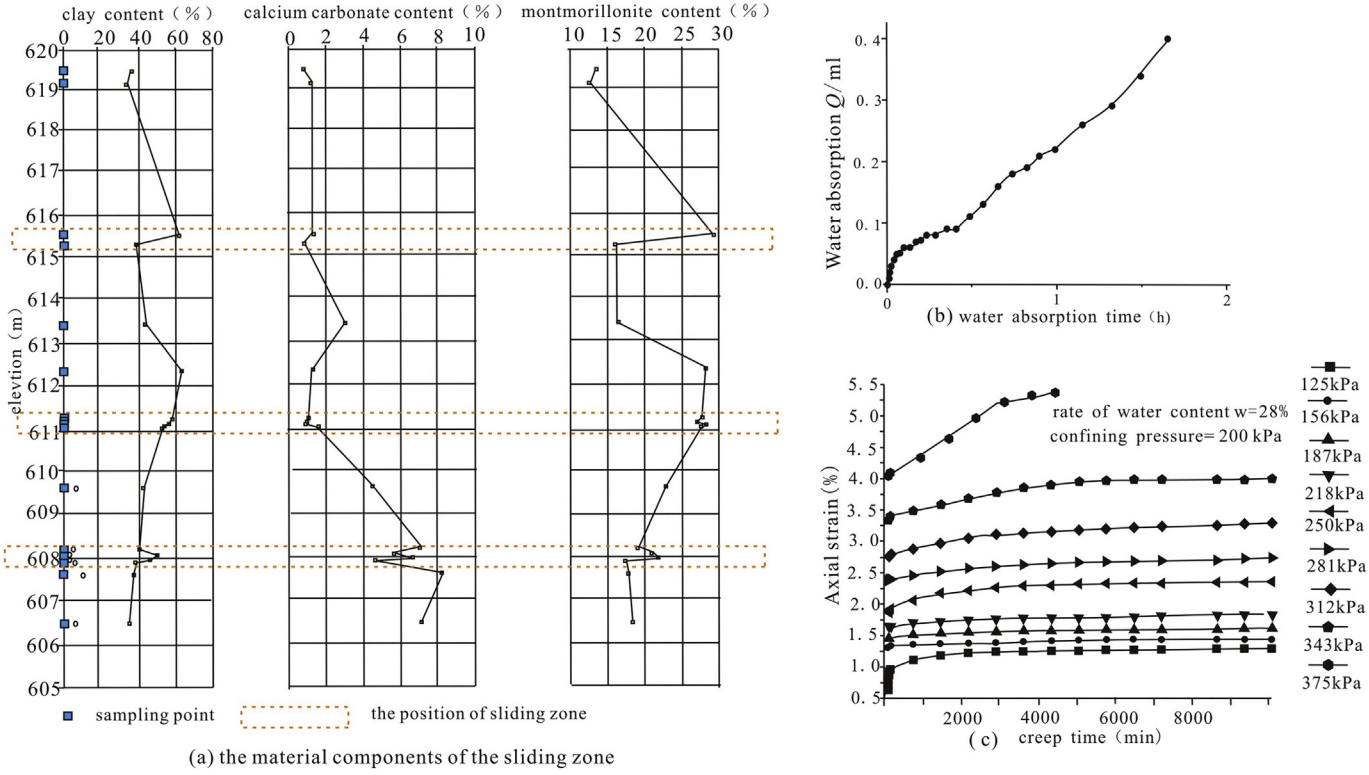

Fig. 6. Characterization of sliding zone in the Bojishan landslide: (a) mineralogy, (b) water absorption, and (c) creep characteristics.

when the rock is subjected to the wetting and drying cycles, which also increases the water seepage. Third, shearing and unloading also form and develop cracks, which allow for water movement. Wetting tests (Fig. 6b) indicate that the total water absorption increases almost linearly with the soaking time (2 h). As water enters the cracks, the cemented claystone expands in areas with high water absorption, which creates more cracks or expands them. Thus, fissures are often observed at locations where different deformation rates are observed, which further facilitates water seepage.

At high clay fractions (e.g., > 50%), the difference between peak and residual strength is clear, and the clay fraction is the controlling factor in sliding shear (Lupini et al., 1981). The clay-rich sliding zone is the result of strain softening and shear localization. Triaxial tests with claystone from the Bojishan landslide produced a peak deviator stress of 1750 kPa under a confining pressure of 400 kPa (Fig. 7a). After the formation of a perforated surface and cracks, shear deformation is observed to evolve along the cracks. The ring shear tests (Fig. 7b) indicate that the residual strength of the Neogene Bojishan claystone is 159 kPa and that the internal friction angle is 11.5° (Xin et al., 2016).

Sliding zones with well-developed cracks and high clay content typically exhibit high viscosities. During long-term creep deformation, the clay particles flow because of high stress, which causes the unordered microstructures to be arranged along the shearing surface. Multi-stage loading creep tests of the remolded soil at a confining pressure of 200 kPa and 28% water content indicate a constant creep rate and accelerated flow and destruction (Fig. 6c). Specifically, during the initial eight loading stages (i.e., 125–343 kPa), the creep strain gradually increases and reaches a constant value after 8000 min.

Table 2
Clay mineralogy in the Neogene claystone and sliding zone.

Sampling number	Location	Particle size < 0.005 mm content (%)	Relative content of clay minerals (%)					Mixed-layer ratio (%)	Absolute content of clay minerals (%)				
			S	I/S	I	K	C		S	I/S	I	K	C
7023	Changshougou landslide	27.64	/	69	20	5	6	75	/	19.1	5.6	1.4	1.7
6910	Bojishan landslide	63.52		69	21	7	6	80	/	50.1	13.2	4.4	3.8
6914		61.36	/	69	22	5	4	65	/	40.1	12.8	2.9	2.3
6749	Caijiapo landslide	50.36	/	73	19	5	3	65	/	36.8	9.6	2.5	1.5
6905	Chendongpo landslide	43.76	/	66	27	4	3	55	/	26.2	10.7	1.6	1.2
7028	Hanjiashan landslide	53.96	/	48	28	11	13	65	/	25.9	15.1	5.9	7.0
7085	Panan landslide	38.24	/	38.5	45.2	0	16.3	35	/	24.87	18.02	0	10.53
7086		63.51	/	34.5	47.3	0	18.2	30	/	13.76	17.13	0	7.26
7087	Saleshan landslide	38.13		40.0	48.6	0	11.4	45	/	14.49	31.70	0	4.13
7088		66.10		31.80	56.8	0	11.4	30	/	20.74	38.52	0	7.44

Notes: I—lllite; I/S—lllite/montmorillonite mixed-layer mineral; C—Chlorite; K—Kaolinite mixed-layer ratio is the percentage of the montmorillonite crystal layer in a mixed-layer mineral.

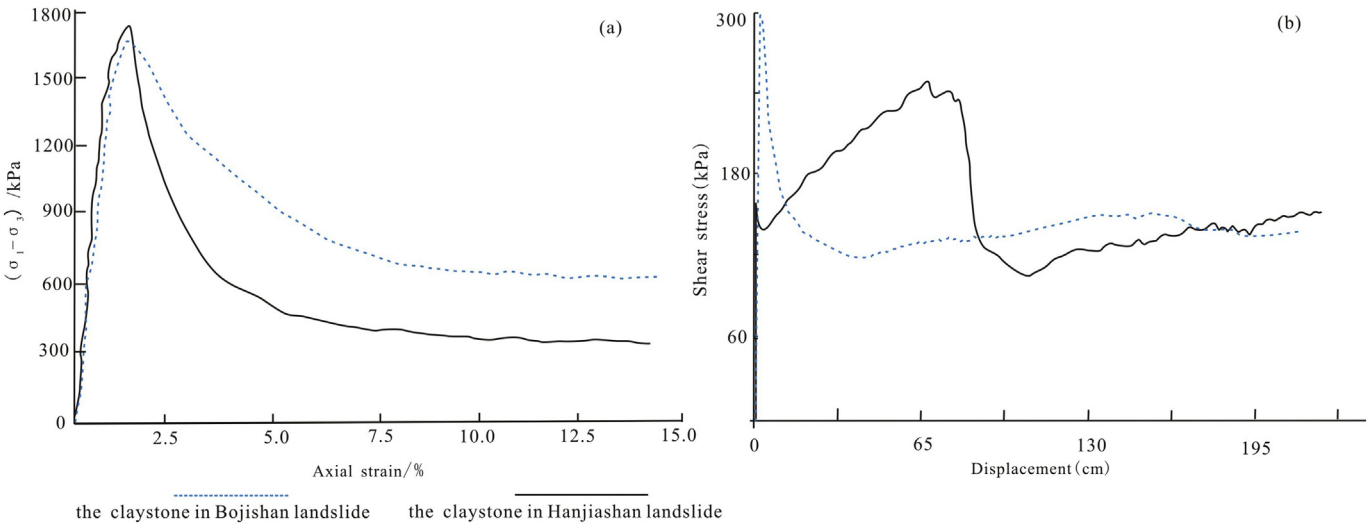

Fig. 7. Triaxial compression: (a) ring shear, and (b) test results for the Neogene claystones.

However, during the ninth loading stage (i.e., 375 kPa), the creep deformation increases continuously and at a higher rate than that in the initial eight stages after 3000 min. The soil microstructure responds to the high vertical load by no-cracking expansion and by the viscous flow of clay minerals, gradually contributing to the accumulated macro-deformation. From the creep test results, it can be observed that clay-rich soils exhibit an internal friction angle of 6.3° and a cohesion of 5.11 kPa.

4.3. Slope deformation and horizontal stress

The temporal and spatial distribution and the intensity attenuation of rotational horizontal landslides in the study area are closely related to the horizontal stresses. The boundary of the Neogene Basin in the northeastern margin of the Qinghai-Tibet Plateau is controlled by the strike-slip faults. The nearly horizontal tectonic stress on the boundary controls the regional geomorphology, i.e., the valley morphology, the stress distribution on the valley slopes, and the geometry of the landslides. For example, the maximum horizontal ground stress near the Tianshui Basin at 492.5 m above sea level is 3.91 MPa, and the vertical stress is 2.13 MPa, whereas the maximum horizontal ground stress at 452 m above sea level is 5.4 MPa, and the vertical stress is 3.2 MPa. The average ratio of horizontal tectonic stress to vertical stress is 1.4. The rapid rise of the Qinghai–Tibet Plateau produced U-shaped valleys that differ from the steephead valleys at the eastern border of the plateau.

The staged river erosion gradually unloads the claystone riverbank slopes. In the profile of Majiabao slope along the Wei River, it is noticed that the fifth terrace of the Wei River was formed at approximately 1.2 Ma BP. The fourth terrace was formed at approximately 0.8 Ma BP, and the height of the slope in the valley reached 40 m. The third and second terraces in the Wei River Valley exhibited slopes that reached heights of 120 and 180 m, respectively. To simulate the stress adjustment in slope that is responsible for the lateral erosion in the Wei River Valley under horizontal stress, the aforementioned deep stress measurements and the FLAC3D 3.0 software were used. The numerical model of Majiabao slope (Fig. 8a) is established with the aid of the measured topography. The slope comprises Neogene claystone, and the constitutive model of the rock mass is an elastic–plastic model. Horizontal stress which is the product of the structural stress multiplier and gravity is applied at each side of the model. The fixed displacement constraint is applied at the bottom boundary. The mechanical parameters in this model are shown in the Fig. 8b.

Fig. 9a exhibits the numerical modeling of the erosion and the stress distribution using the U-shaped valley surface in the Baoji section of the middle reach of the Wei River. The results indicate that the initial unloading depth is shallow and that the plastic zone exhibited a curved surface when the fourth and the third terrace appeared in Fig. 9a. With increasing lateral erosion, the plastic deformation owing to shear stress

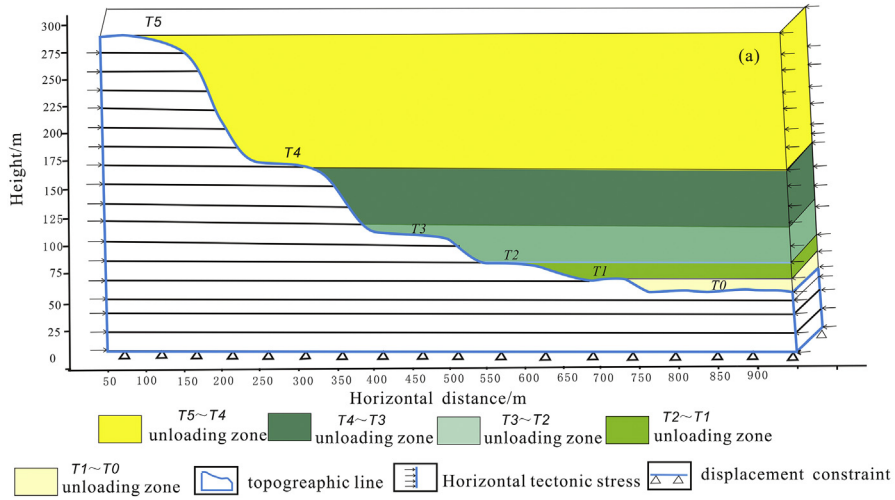

(b) Calculation parameters

density	2130 kg/m^3
cohesion	102.5 kPa
internal friction angle	21°
tensile strength	215kPa
Modulus of elasticity	2.3MPa

Fig. 8. The numerical model of Majiabao slope across the Wei River: (a) the boundary condition and calculation process; and (b) parameters.

expanded to the rear margin (L shape in Fig. 9b). The horizontal shear stress is the major cause for the plastic deformation that is observed in the sliding band at the bottom of the slope after the formation of the second terrace. This result is consistent with the results of the in-situ test that have been reported in literature (James, 2001). In shale, the horizontal shear stress owing to river erosion is 150% of the vertical stress, and the horizontal normal stress is 50% higher than the overburden pressure.

5. Discussion and conclusions

5.1. Discussion

Movement and deformation is an irreversible process in case of a landslide. The coupling of the tectonic activity and the mechanical properties of rock and soil controlled the development of rotational-translational landslides. These landslides fail along the bedding parallel shear zone.

The coupling of the tectonic activity and the mechanisms of rock and soil controlled the development of rotational–translational landslides. These landslides fail along clear sliding zones.

The temporal and spatial distribution of the rotational–horizontal landslides at the northeastern margin is related to the horizontal stress environment of the region and the lateral erosion of the rivers. Landslides respond to regional tectonics. The rotational–translational landslides in the Neogene basins of the northeastern margin are good examples of the response to tectonics. Furthermore, the horizontal shear stress is responsible for the plastic deformation and shearing parallel to bedding.

The application of horizontal shear stress gradually breaks and weakens the claystones. When the overconsolidated claystone dilates due to shear, pores and cracks are observed to form, which increase the water seepage and accelerate the deformation and connection of cracks. Furthermore, the recovery of the strain energy in claystone rearranges the clay minerals and increases the water content. The creep in the sliding zone, expansion of cracks, and increase in moisture caused by the underground water promote the flow deformation of materials, and the sliding surface will favor the formation of layers with high clay and low calcium carbonate content. Illite–montmorillonite clays in the main sliding zones increase the water absorption and sensitivity. The strong water-holding capacity reduces the friction coefficient in the sliding zone, decreases the soil viscosity, and increases the soil flow.

Earthquakes, groundwater, and gravitational creep produce horizontal stresses that trigger the landslides (Zhang et al., 2016; Zhang and Yin, 2013). When the pore-water pressure fluctuates, the deformation of the sliding zones accelerates, and the stability of landslides

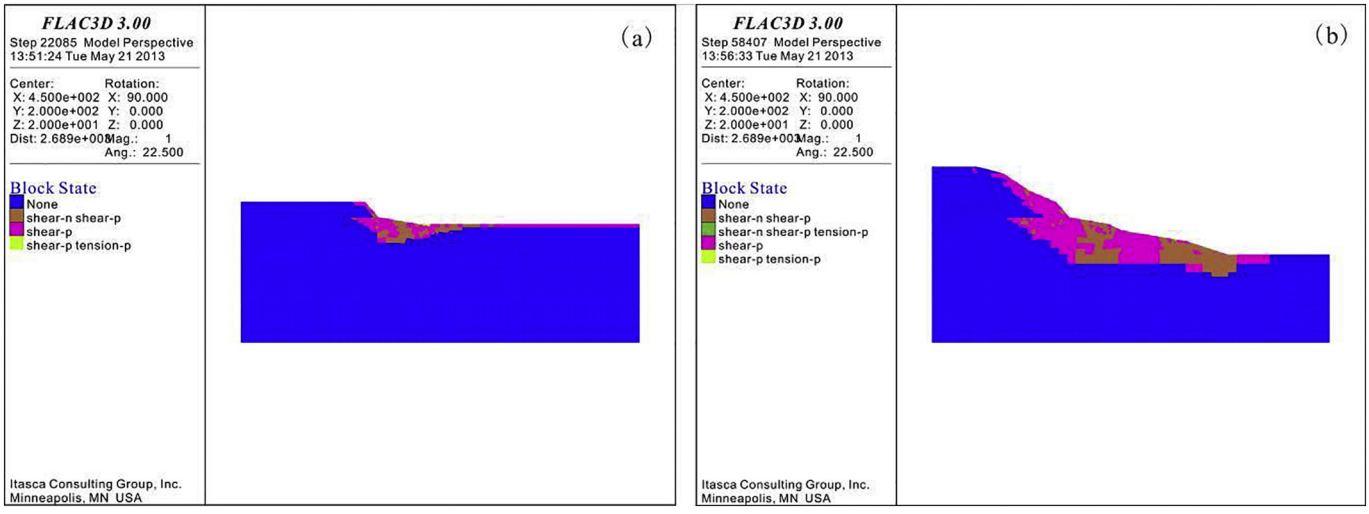

Fig. 9. Stress variation in the slope at the valley bottom of the Wei River Stress state when the fourth terrace appeared; (b) stress state of the slope when the second terrace appeared.

depends on the strength of the nearly horizontal shear zone.

5.2. Conclusions

Landslides have occurred at several locations since the late Pleistocene, and they are good indicators of the regional tectonic and geomorphological processes. Rotational–translational landslides are common in the northeastern margin of the Qinghai–Tibet Plateau near the Neogene basins. Their activity is affected by the uplift of the Qinghai–Tibet Plateau. The bedding-parallel shear zones in rotational–translational landslides developed in the overconsolidated Pliocene mudstones that depict high clay content. Erosion leads to the development of nearly horizontal shear stresses in the sliding masses that are characterized by low internal friction angle materials ($< 10°$).

The bedding-parallel shear zones are located within the weak layers that depict high clay and low calcium contents. The hydration and creep deformation of clay minerals provide the driving forces for landslides. The horizontal shearing is accelerated by the increasing pore-water pressure and creep.

Acknowledgments

This study was supported by the National Science Foundation of China (Grant No. 41402281 and 41372374) and the Geological Survey Project (No. DD20160271). We wish to thank Professor Jinliang Han and the Geological Disaster Monitoring Station in Baoji City for providing the data related to the Bojishan landslide.

References

Carey, J.M., Petley, D.N., 2014. Progressive shear-surface development in cohesive materials; implications for landslide behaviour. Eng. Geol. 177, 54–65.
Di Maio, C., Vassallo, R., Vallario, M., 2013. Plastic and viscous shear displacements of a deep and very slow landslide in stiff clay formation. Eng. Geol. 162, 53–66.
Di Maio, C., Vassallo, R., Vallario, M., Pascale, S., Sdao, F., 2010. Structure and kinematics of a landslide in a complex clayey formation of the Italian Southern Apennines. Eng. Geol. 116, 311–322.
Hart, M.W., 2000. Bedding parallel shear zones as landslides mechanisms in horizontal sedimentary rocks. Environ. Eng. Geosci. 2, 95–113.
Haruo, S.Z., 2001. Process of slip-surface development and formation of slip-surface clay in landslides in Tertiary volcanic rocks, Japan. Eng. Geol. 68, 289–317.
James, V.H., 2001. Discussion on “Bedding parallel shear zones as landslides mechanisms in horizontal sedimentary rocks”. Environ. Eng. Geosci. 2, 217–219.
Kimuta, S., Kaneko, H., Noda, S., Ito, T., Minagawa, H., 2018. Shear-induced permeability reduction and shear-zone development of sand under high vertical stress. Eng. Geol. 238, 86–98.
Lupini, J.F., Skinner, A.E., Vaughan, P.R., 1981. The drained residual strength of cohesive soils. Geotechnique 31 (2), 181–213.
Massey, C.I., Petley, D.N., Mcsaveney, M.J., 2013. Patterns of movement in reactivated landslides. Eng. Geol. 159, 1–19.
Massey, C.I., Petley, D.N., Mcsaveney, M.J., Archibald, G., 2016. Basal sliding and plastic deformation of a slow, reactivated landslide in New Zealand. Eng. Geol. 208, 11–28.
Palladino, D.J., Peck, R.B., 1972. Slope failure in an overconsolidated clay, Seattle, Washington. Geotechnique 22 (4), 563–595.
Petley, D.N., Bulmer, M.H., Murphy, W., 2002. Patterns of movement in rotational and translational landslides. Geology 30, 719–722.
Skempton, A.W., 1964. Long term stability of clay slopes. Geotechnique 14 (2), 75–101.
Skempton, A.W., 1985. Residual strength of clays in landslides, folded strata and the laboratory. Geotechnique 35 (1), 3–18.
Varnes, D.J., 1978. Slope movement types and processes. In: Schuster, R.L., Krizek, R.J. (Eds.), Landslides, Analysis and Control. 176. Transportation Research Board, National Academy of Sciences, Special Report, Washington, DC, pp. 11–33.
Wen, B.P., Aydin, A., 2003. Microstructural study of a natural slip zone, quantification and deformation history. Eng. Geol. 68, 289–317.
Xin, P., Liang, C.Y., Wu, S.R., Liu, Z., Shi, J.S., Wang, T., 2016. Kinematic characteristics and dynamic mechanisms of large-scale landslides in a loess plateau: a case study for the north bank of the Baoji stream segment of the Wei River, China. Bull. Eng. Geol. Environ. 75, 659–671.
Yenes, M., Monterrubio, S., Nespereira, J., Santos, G., 2009. Geometry and kinematics of a landslide surface in tertiary clays from DueroBasin (Spain). Eng. Geol. 104, 41–54.
Yenes, M., Monterrubio, S., Nespereira, J., Santos, G., Fernandez-Macarro, B., 2015. Large landslides induced by fluvial incision in the Cenozoic Duero Basin (Spain). Geomorphology 246, 263–276.
Zhang, M., Yin, Y., 2013. Dynamics, mobility-controlling factors and transport mechanisms of rapid long-runout rock avalanches in China. Eng. Geol. 167, 37–58.
Zhang, Y., Cheng, Y., Yin, Y., Lan, H., Wang, J., Fu, X., 2016. High-position debris flow: A long-term active geohazard after the Wenchuan earthquake. Eng. Geol. 180, 45–54.
Zhang, Z., Wang, T., Wu, S., Tang, H., Liang, C., 2017a. The role of seismic triggering in a deep-seated mudstone landslide, China: Historical reconstruction and mechanism analysis. Eng. Geol. 226, 122–135.
Zhang, Z., Wang, T., Wu, S., Tang, H., Liang, C., 2017b. Seismic performance of loess-mudstone slope in Tianshui-Centrifuge model tests and numerical analysis. Eng. Geol. 222, 225–235.
Zhang, Z., Wang, T., Wu, S., Tang, H., Liang, C., 2018. Dynamics characteristic of red clay in a deep-seated landslide, Northwest China: an experiment study. Eng. Geol. 239, 254–268.